Chin. J. Astron. Astrophys. Vol. 5 (2005), No. 1, 49–56
(*http://www.chjaa.org*)

Chinese Journal of
Astronomy and
Astrophysics

Images at 20 cm and the Spectrum Index of NGC 2997 *

Hui Men and Jin-Lin Han

National Astronomical Observatories, Chinese Academy of Sciences, Beijing 100012;
mh@bao.ac.cn

Received 2004 April 29; accepted 2004 July 1

Abstract We present total intensity maps of the galaxy NGC 2997 at frequencies 1435.1 MHz (λ21 cm) and 1652.4 MHz (λ18 cm) observed with the Very Large Array (VLA). The high spatial resolution allows us to distinguish two dominant arms. Using multi-frequency data, we separate the thermal and non-thermal contributions to the radio emission. The thermal emission is about 35% of the total emission at λ3 cm. We use it to estimate a space-averaged thermal electron density, $\langle n_{\rm e}\rangle \sim 0.049$ cm^{-3}. The spectral index map shows that the optical arms and the central part of the galaxy have flatter spectra. We also determine the flux densities of 22 radio sources in the field-of-view of 25′.

Key words: galaxies: individual (NGC 2997) — galaxies: ISM — galaxies: spiral — radio continuum: galaxies

1 INTRODUCTION

NGC 2997 ($\alpha = 09^{\rm h}45^{\rm m}38.8^{\rm s}$; $\delta = -31°11'28''$) is a bright late-type galaxy which has "hot spot" emission regions surrounding the nucleus (Peterson 1978; Marcelin et al. 1980). Optically, the galaxy possesses two dominant spiral arms, one of which branches prominently westward into a third arm (Block et al. 1994). The very sharp and symmetric arms of this galaxy are consistent with a typical Sc galaxy with no obvious interacting companion (Milliard & Marcelin 1981). The distance of NGC 2997 is about 13.8 Mpc ($H_0 = 75\,{\rm km\,s^{-1}}$ Mpc^{-1}, Maoz et al. 1996), so 1 arcmin corresponds to 4.0 kpc. The galaxy has an inclination angle of $i = 40°$ and a mean pitch angle of 13.7° for the spiral arms (Milliard & Marcelin 1981; Garcia-Gomez & Athanassoula 1993). The southern arm is the closer one to the observer, so, HII regions appear brighter in this arm than in the northern arm.

The far-infrared-radio correlation of NGC 2997 was studied by Fitt et al. (1992) with its first radio continuum observation at 1.49 GHz by Condon (1987), in which the spiral arms were barely resolved. Han et al. (1999) derived the regular magnetic fields of NGC 2997 by multi-band radio observations. At the inner edge of the arms, the regular field is about 8 μG.

∗ Supported by the National Natural Science Foundation of China.

Radio continuum emission of spiral galaxies consists of two components: a non-thermal synchrotron emission and a thermal free-free emission (Niklas et al. 1997). The two components can be separated by fitting a model of free-free and non-thermal synchrotron emission to the spectrum of the galaxy. However, previous investigations of NGC 2997 did not give any information on the spectral index of the non-thermal emission or the electron density distribution.

In this paper, we processed our data of NGC 2997 observed with the VLA at 1435.1 MHz (λ21 cm) and 1652.4 MHz (λ18 cm) to produce total intensity maps. The spiral arms can be clearly resolved in both maps. Together with data at λ3 cm and λ6 cm, we separate the thermal and non-thermal emissions and derive the value of the space-averaged electron density $\langle n_{\rm e}\rangle$ in NGC 2997. We also identify 22 radio sources within $25'$ around NGC 2997. In Sect. 2 we present the observation, in Sect. 3 we describe the results, and in Sect. 4 we provide a brief discussion.

2 OBSERVATIONS AND DATA REDUCTION

The observation was carried out on 1998 Nov. 12, using the Very Large Array (VLA) in its BnC array at 1435.1 MHz and 1652.4 MHz. The bandwidths at the two frequencies are 50 MHz and 25 MHz, respectively. The BnC array was chosen so as to obtain a sufficiently high resolution ($15''$) to resolve the spiral arms and the central part. The total on-source integration time was 186 minutes. The flux density scale was calibrated by 3C138. A nearby strong source J1018−317 was used as a phase calibrator.

A standard procedure in AIPS was used in the data reduction. The calibrators' flux densities were calculated by SETJY for 3C 138 (8.2707 Jy at 1435.1 MHz and 7.6002 Jy at 1652.4 MHz), GETJY for J1018−317 (3.5371 Jy at 1435.1 MHz and 3.2124 Jy at 1652.4 MHz) and set in the SU table. Being aware of the zero-spacing problem, we set five values, 0.5, 0, 0, 0 and 20000, for ZEROSP in task IMAGR according to the visibility sample when we made the total intensity maps. After a few iterations for the clean and self–calibration, we obtained the total intensity maps at the two frequencies. The primary beam attenuation was corrected by using the task PBCOR. Finally, we used IMSTAT to obtain the flux densities of NGC 2997 and other sources in the field-of-view covered by this observation.

3 RESULTS

3.1 Total Intensity Maps

We present the total intensity maps at 1435.1 MHz and 1652.4 MHz overlaid on an optical image in Fig. 1 and Fig. 2. The distribution of the radio continuum emission is roughly similar to the optical pattern with two dominant arms, but is more extended than the region of the optical arms. Obvious differences between the radio and optical images are a gap near $\alpha = 09^{\rm h}45^{\rm m}33^{\rm s}$; $\delta = -31^\circ10'$ and a bright point at $\alpha = 09^{\rm h}45^{\rm m}39.9^{\rm s}$; $\delta = -31^\circ08'50.0''$ north of the galaxy, which appears to be a non-thermal background source because of the absence of a bright optical counterpart.

In our two total intensity maps, the position of the central source is $\alpha = 09^{\rm h}45^{\rm m}38.6^{\rm s}$; $\delta = -31^\circ11'26.0''$ (J2000). The uncertainty in α and δ is $0.3^{\rm s}$ and $4.0''$, respectively. The position is close to values in Han (1999): $\alpha = 09^{\rm h}45^{\rm m}38.7^{\rm s}$; $\delta = -31^\circ11'27''$, de Vaucouleurs et al. (1991): $\alpha = 09^{\rm h}45^{\rm m}39.4^{\rm s}$; $\delta = -31^\circ11'28''$. The galaxy covers an area of $6.3'$ by $5.8'$. In this area, the integrated flux density is 195±11.8 mJy at λ21 cm and 128±15.6 mJy at λ18 cm, thus the integrated flux density at λ18 cm is much weaker than that at λ21 cm. In these two bands,

the integrated flux density indicates that the northern arm is brighter than the southern arm, in contradiction with the situation for the HII regions.

Note that the zero-space uv coverage is missing in VLA observations, which impacts on the determination of the flux density of the large-scale component for the extent sources, and could not be corrected completely by the AIPS procedure. We checked the uv data and estimated that there are 5% zero-spacing flux densities missed in each band.

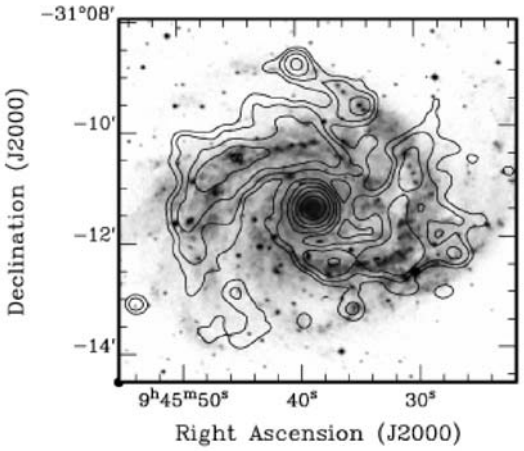

Fig. 1 Total intensity map at 1435.1 MHz (λ21 cm) with a resolution of 19″, superimposed onto an optical image from the Digitized Sky Survey. Contours: (–3, 3, 6, 12, 24, 48 and 96)×σ. The rms σ is 98 μJy per beam area.

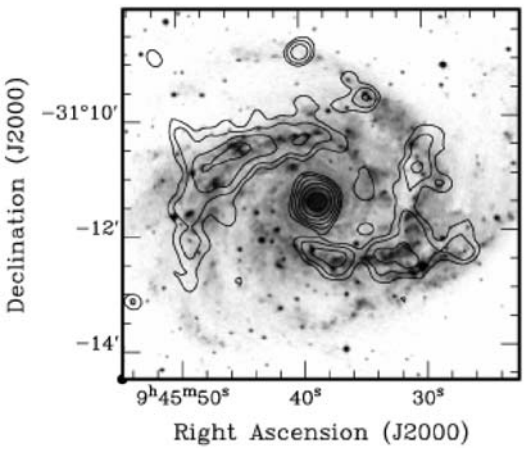

Fig. 2 Total intensity map at 1652.4 MHz (λ18 cm) with a resolution of 18″, superimposed onto an optical image from the Digitized Sky Survey. Contours: (–3, 3, 6, 12, 24, 48 and 96)×σ. The rms σ is 111 μJy per beam area.

3.2 Separation of Thermal and Non-thermal Emissions

For the thermal free-free radiation in the optically thin region, $S_\nu^{\rm th} \propto \nu^{-0.1}$. If synchrotron and Compton losses are not too strong, the non-thermal emission follows a power law (Niklas et al. 1997). By including the flux densities of 67±11 mJy at λ6 cm and 34±4 mJy at λ3 cm obtained by Han et al. (1999), we fit the following model to separate the thermal and non-thermal emissions and find the non-thermal spectral index:

$$S_\nu = A\nu^{\alpha_{\rm nt}} + B\nu^{-0.1} \ , \tag{1}$$

where $\alpha_{\rm nt}$ is the non-thermal spectral index. For NGC 2997, the mean integrated radio spectral index is $\alpha_{\rm nt} = -1.12 \pm 0.07$, and the thermal fraction in the total flux density is about 7.3% at λ21 cm, 10.9% at λ18 cm, 18.8% at λ6 cm, and 34.9% at λ3 cm. The value of $\alpha_{\rm nt}$ is a little steeper than the mean value $\langle\alpha_{\rm nt}\rangle = -0.83\pm0.02$ obtained for a sample of 74 galaxies by Niklas et al. (1997). The thermal fraction at λ3 cm agrees with the mean value 35 ± 15% given by Israel & van der Hulst (1983) for a sample of Sc galaxies. The result obtained with our best-fit $\alpha_{\rm nt}$ is shown as the solid line in Fig. 3. We also fitted $\alpha_{\rm nt}$ with the flux densities at λ21 cm, λ6 cm, and λ3 cm, ignoring the flux density at λ18 cm because of its obviously weaker intensity. The best-fit value is $\alpha_{\rm nt} = -1.10$.

Now, we derive the spectral index map. The intensity of the thermal emission is almost the same in the four bands, only a small fraction of the total emission at $\lambda 21$ cm, $\lambda 18$ cm and $\lambda 6$ cm, so we can regard the spectral index of the observed total emission between $\lambda 21$ cm and $\lambda 6$ cm as the spectral index of the non-thermal emission. In practice we use task CONVL in AIPS to smooth out the maps at $\lambda 3$ cm, $\lambda 6$ cm and $\lambda 21$ cm to the same resolution of $19''$. The whole galaxy was covered by 30×30 pixels of $14'' \times 12''$. The spectral index between $\lambda 21$ cm and $\lambda 6$ cm, $\alpha_{21,6}$ is computed only when the observed flux densities for the same pixel in the two maps are greater than 3σ. The distribution of $\alpha_{21,6}$ is shown in Fig. 4(A). With the flux density at $\lambda 6$ cm and the $\alpha_{21,6}$ for non-thermal spectral index, we calculate the non-thermal flux density at $\lambda 3$ cm, and then subtract it from the total flux density of $\lambda 3$ cm to obtain the thermal flux density. The maps of the non-thermal and thermal radio continuum emissions at $\lambda 3$ cm are shown in Figs. 4(B) and (C).

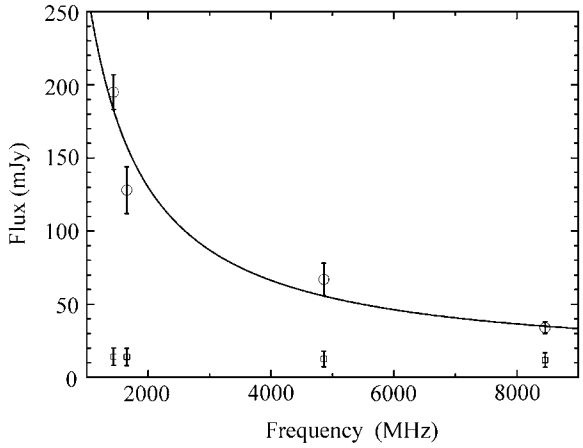

Fig. 3 Integrated flux densities (open circles) of NGC 2997 and the corresponding thermal flux densities (open squares) at our four frequencies. The solid line is a fit of the non-thermal emission to the spectrum with Eq. (1).

3.3 Electron Density in the Disk

The electron density $n_{\rm e}$ can be estimated from the thermal radio flux density $S_{\rm th}$. The mean emission measure of ionized gas is given by:

$$\frac{EM}{\rm pc\ cm^{-6}} = \frac{4.13 S_{\rm th}(\nu)}{\rm mJy\ beam^{-1}} \left(\frac{T_{\rm e}}{\rm K}\right)^{0.35} \left(\frac{\nu}{\rm GHz}\right)^{0.1} \left(\frac{\Theta}{\rm arcmin}\right)^{-2} . \quad (2)$$

Here,

$$EM = \langle n_{\rm e}/{\rm cm^{-3}}\rangle^2 [L/{\rm pc}]/(f \cos i) , \quad (3)$$

and Θ is the half power beam width, $T_{\rm e}$ is the electron temperature. In Eq. (3), L is the depth of the emission region along the line-of-sight, $f = \langle n_{\rm e}\rangle / n_{\rm e}$ is the filling factor, and i is the inclination angle of the galaxy. For NGC 2997, we take the observed HPBW value of $15''$, i.e., $\Theta = 0.25$. The mean percentage of thermal emission is 35% at $\lambda 3$ cm, so $S_{\rm th} =$

0.018 mJy beam^{-1}. We can assume an electron temperature of $T_{\rm e} = 8000\,{\rm K}$, a typical value of the warm ionized gas in our Galaxy and reasonable for general spiral galaxies (Reynolds 1985). Using Eq. (2), we obtain $EM = 34.4\ {\rm pc\,cm^{-6}}$. After correcting for the inclination $i = 40^\circ$ (Milliard & Marcelin 1981), we have $EM = 24.3\ {\rm pc\,cm^{-6}}$. When the thermal emission is coming from a thin disk and a thick disk, Eq. (3) is changed to

$$\langle n_{\rm e}\rangle = \sqrt{EM \cdot \cos i/(L_1/f_1 + L_2/f_2)}\ , \tag{4}$$

where $\langle n_{\rm e}\rangle$ is the mean electron density of the two disks, L_1 and f_1 are the thickness and the filling factor of the thin disk, and L_2 and f_2 are those of the thick disk. NGC 2997 is an Sc galaxy (Milliard et al. 1981), similar to our Galaxy. So, we can take the filling factor and thickness of our Galaxy,

$$L_1 = 140\,{\rm pc}\ , \quad f_1 = 0.038\ ,$$
$$L_2 = 1800\,{\rm pc}\ , \quad f_2 = 0.25\ ,$$

(Reynolds 1991; Ferrière 2001; Berkhuijsen 1998; Reynolds 2004) to calculate the mean electron density distribution of NGC 2997. Using its observed thermal emission at $\lambda 3\,{\rm cm}$, we can calculate its mean electron density distribution using Eq. (2) and Eq. (4). The result is shown in Fig. 4(D) for the pixels where the thermal flux density is not zero. For the average over the whole galaxy, we obtain $\langle n_{\rm e}\rangle \simeq 0.049\,{\rm cm^{-3}}$.

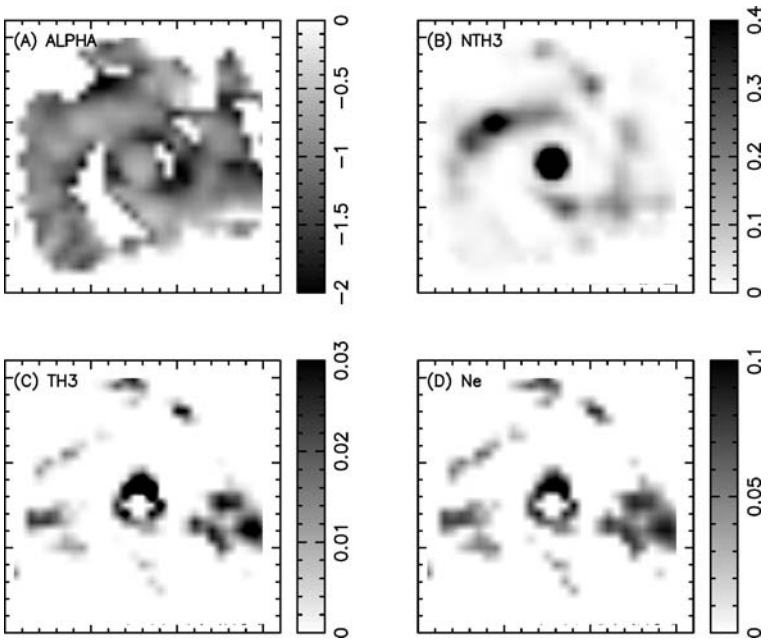

Fig. 4 Images of NGC 2997. (A) Spectral index map of $\alpha_{21,6}$. (B) Map of non-thermal continuum emission (mJy). (C) Map of thermal continuum emission (mJy). (D) Distribution of electron density (cm^{-3}). The size of every image is $7' \times 6'$.

3.4 Other Sources

Our observation has a field of view of 25′. NGC 2997 is located at the center, and covers 6.3′. Besides NGC 2997, there are nearly two dozens of bright points in the field (Fig. 5). We identify 22 radio sources from the NASA/IPAC Extragalactic Database (NED). These are summarized in Table 1. Col. 2 lists the NED name, Cols. 3 and 4, the position determined from our map at 1435.1 MHz, and Cols. 5, 6 and 7, the NVSS flux density (from Condon et al. 1998) and at two of our frequencies. The positions of these sources are slightly different from the values given by NED. We note that the compact D and CnD configurations of the VLA used for the NVSS produce a map of resolution of 45″ and the rms brightness $\sigma \approx 0.45\,\mathrm{mJy\,beam^{-1}}$. The survey was based on snapshot observations (Condon et al. 1998). In comparison, the resolution of our map is 19″, and sensitivity is about $\sigma \approx 98\,\mu\mathrm{Jy\,beam^{-1}}$, because the integration time of our observation is 186 minutes which leads to a better uv coverage and hence a higher signal-to-noise ratio.

Table 1 22 Radio Sources in the Field of View

Num.	Object Name	RA (2000)	DEC (2000)	S_{NVSS}	$S_{1435.1\,\mathrm{MHz}}$	$S_{1652.4\,\mathrm{MHz}}$
		h m s	° ′ ″	mJy	mJy	mJy
(1)	(2)	(3)	(4)	(5)	(6)	(7)
1	NVSS J094417−305744	09 44 17.5	−30 57 40	15.8	13.3±0.9	15.1±0.9
2	NVSS J094432−305850	09 44 32.4	−30 58 49	21.9	18.8±0.9	17.5±0.9
3	TXS 0942−306	09 44 46.7	−30 55 37	95.1	90.6±1.5	85.1±1.6
4	NVSS J094440−310824	09 44 40.7	−31 07 21	13.5	14.1±0.4	13.2±0.4
5	NVSS J094444−311918	09 44 44.6	−31 19 09	22.4	19.9±0.4	18.8±0.4
6	NVSS J094445−312435	09 44 46.4	−31 24 21	4.2	3.0±0.2	2.6±0.2
7	NVSS J094458−311345	09 44 59.0	−31 13 46	2.6	3.3±0.2	2.9±0.2
8	NVSS J094458−311007	09 44 59.0	−31 10 02	2.3	3.5±0.2	3.1±0.2
9	2MASX J09445696−3112458	09 44 57.2	−31 12 42		0.7±0.2	0.7±0.2
10	NVSS J094500−310141	09 44 59.7	−31 01 58	2.7	1.3±0.2	1.7±0.2
11	NVSS J094501−310312	09 45 01.3	−31 03 25	10.0	3.0±0.5	3.2±0.5
12	PMN J0945−3057	09 45 32.4	−30 57 58	205.7	204.5±1.7	188.6±1.8
13	NVSS J094535−312012	09 45 35.8	−31 20 06	74.1	69.4±0.9	64.4±0.5
14	NVSS J094549−312613	09 45 48.9	−31 26 02	15.1	11.6±0.5	12.9±0.3
15	NVSS J094549−310618	09 45 49.8	−31 06 22	35.5	32.1±0.8	28.7±0.4
16	2MASX J09461564−3114038	09 46 15.4	−31 14 02	7.7	10.0±0.6	9.6±0.3
17	NVSS J094617−305407	09 46 18.1	−30 54 10	30.2	27.5±1.2	24.9±2.7
18	NVSS J094618−305049	09 46 18.1	−30 50 50	20.0	17.0±0.7	15.6±1.6
19	NVSS J094653−310532	09 46 53.0	−31 05 17	7.2	2.6±0.3	2.3±0.3
20	NVSS J094659−310209	09 46 59.2	−31 02 00	24.0	19.1±0.9	16.9±0.7
21	NVSS J094700−310323	09 47 00.2	−31 03 16	31.6	24.9±1.0	23.9±0.9
22	NVSS J094704−310856	09 47 03.7	−31 08 48	5.9	6.2±0.5	5.4±0.4

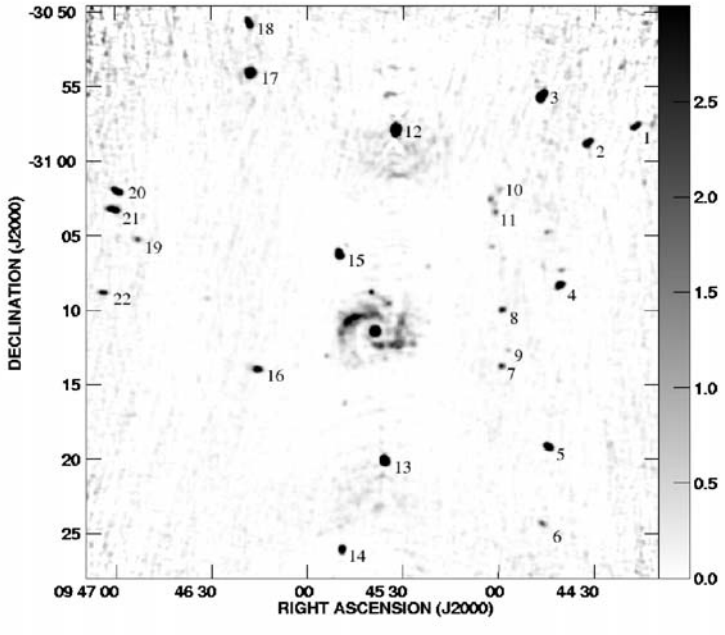

Fig. 5 22 sources are marked in the field of more than $25'$. These sources are listed in Table 1.

4 DISCUSSION

If relativistic electrons can escape very easily and have no time to undergo energy losses, the emission intensity will have a flat spectrum. However, if cosmic-rays are well confined, synchrotron and inverse Compton losses will strongly affect the relativistic electron population and steepen the synchrotron spectrum. Niklas et al. (1997) pointed out that galaxies with a strong star formation activity have a flatter non-thermal spectrum.

Figure 4(A) shows a two-dimensional map of the spectral index of NGC 2997. At the edge of the radio arms, especially at the inner edge, the radio emission spectrum is steeper than in the optical spiral structure. This may be due to two causes. In the optical arm regions, the high star formation rate leads to a large amount of dust and hot stars, and produces much thermal emission, which flattens the spectrum. On the other hand, regular magnetic fields along the inner edge of the spiral arms (Han et al. 1999) can confine the nearby relativistic electrons and produce more non-thermal emission at a radio frequency with a steeper spectrum.

At the radio band, thermal emission mainly comes from gases with an electron temperature $T_{\rm e} \sim 10^4$ K. We noticed that on the thermal flux density map at $\lambda 3$ cm (Fig. 4(C)) there are two regions where the thermal flux density is very strong: one is the area surrounding the nucleus, and the other is in the middle of the west arm where the arm is split into two parts. The central one is probably due to the fact that there is a bubble-like HII region surrounding the nucleus (Marcelin et al. 1980). The thermal emission near the arm bifurcation can also result from star formation in that area.

5 CONCLUSIONS

We have obtained total intensity maps of NGC 2997 at both 1435.1 MHz and 1652.4 MHz. The spiral structure is clearly resolved. By separating thermal and non-thermal radio emissions, we derived the mean values of the non-thermal spectral index and electron density. Using the spectral index between $\lambda 21$ cm and $\lambda 6$ cm for $\alpha_{\rm nt}$, we obtained maps of the spectral index and of the thermal emission at $\lambda 3$ cm, and then used the emission map to calculate an electron density map. Finally, we determined the flux densities of 22 radio sources in the same field.

Acknowledgements We thank Dr. Katia Ferrière and the referee, Dr. J. H. Zhao, for careful reading of the paper and useful suggestions, which greatly help to improve the presentation. J. L. Han is supported by the National Natural Science Foundation of China (10025313) and the National Key Basic Research Science Foundation of China (G19990754) as well as the partner group of MPIfR at NAOC. The Digitized Sky Survey data were taken by the Royal Observatory Edinburgh and produced at the Space Telescope Science Institute. The National Radio Astronomy Observatory is a facility of the National Science Foundation operated under cooperative agreement by Associated Universities, Inc.

References

Berkhuijsen E. M., 1998, In: D. Breitschwerdt, M. J. Freyberg, J. Truempered, eds., IAU Colloq. No. 166, Vol. 506, Lecture Notes in Physics, p.301
Block D. L., Bertin G., Stockton A. et al., 1994, A&A, 288, 365
Condon J. J., 1987, ApJS, 65, 485
Condon J. J., Cotton W. D., Greisen E. W. et al., 1998, AJ, 115, 1693
de Vaucouleurs G., de Vaucouleurs A., Corwin H. G. Jr. et al., 1991, Third Reference Catalogue of Bright Galaxies, Berlin: Springer
Ferrière K. M, 2001, Reviews of Modern Physics, 73, 1031
Fitt A. J., Howarth N. A., Alexander P. et al., 1992, MNRAS, 255, 146
Garcia-Gomez C., Athanassoula E., 1993, A&AS, 100, 431
Han J. L., Beck R., Ehle M. et al., 1999, A&A, 348, 405
Israel F. P., van der Hulst J. M., 1983, AJ, 88, 1736
Marcelin M., Comte G., Courtes G. et al., 1980, PASP, 92, 38
Milliard B., Marcelin M., 1981, A&A, 95, 59
Maoz D., Barth A. J., Sternberg A. et al., 1996, AJ, 111, 2248
Niklas S., Klein U., Wielebinski R., 1997, A&A, 322, 19
Peterson C. J., 1978, ApJ, 226, 75
Reynolds R. J., 1985, ApJ, 294, 256
Reynolds R. J., 1991, In: IAU Symp. 144th, The interstellar disk-halo connection in galaxies, p.67
Reynolds R. J., 2004, Advances in Space Research, 34, 27